Dynamic Behavior of Imperfect FGM Beams with Various Porosity Distribution Rates: Analysis and Modeling

Lazreg Hadji, Vagelis Plevris, and Royal Madan

Contents

1 Introduction

Functionally graded materials (FGMs) signify a significant advancement in engineering and scientific domains, offering solutions to intricate challenges encountered across diverse industries, notably aerospace and biomedical applications [1–3]. It is crucial to recognize that porosities may arise within FGMs during the sintering phase of fabrication, mainly because of the differences in solidification temperatures between the different materials [4, 5]. In the design of FGM structures exposed to dynamic loads, accounting for the influence of porosity is paramount [6, 7]. The

L. Hadji
University of Tiaret, Tiaret, Algeria

Laboratory of Geomatics and Sustainable Development, University of Tiaret, Tiaret, Algeria
e-mail: lazreg.hadji@univ-tiaret.dz

V. Plevris (✉)
Qatar University, Doha, Qatar
e-mail: vplevris@qu.edu.qa

R. Madan
Graphic Era (Deemed to be University), Dehradun, India

M. Kioumarsi, B. Shafei (eds.), *The 1st International Conference on Net-Zero Built Environment*, Lecture Notes in Civil Engineering 237,
https://doi.org/10.1007/978-3-031-69626-8_126

disparity in solidification temperatures between metals and ceramics gives rise to the formation of metal phase grains, while ceramics persist as interspersed particles. Furthermore, the varied sizes and configurations of the reinforcement (ceramics) powders can engender pore formation in proximity to the reinforced particles, leading to divergent levels of porosity within both phases [6].

This investigation examines the repercussions of distinct porosity types within both ceramic and metal constituents. Each discussed porosity type manifests differing percentages of porosity in ceramic and metal phases. The analysis encompasses how the stiffness of functionally graded beams is affected by the power-law index, furnishing elucidations into their dynamic response. Furthermore, scrutiny of the length-to-thickness ratio yields significant insights into the ramifications of geometric proportions. Collectively, this study offers novel insights into the behavior of porous functionally graded beams, considering a spectrum of parameters and underscoring their relevance in real-world applications.

2 Problem Formulation

2.1 Constitutive Relations of FG Beams Made of Metal and Ceramic

We examine an imperfect FGM characterized by the porosity volume fraction, a (where $a \ll 1$), evenly distributed between the two constituents. The rule of mixture (modified), as proposed by [8], is

$$P = P_m\left(V_m - \frac{\alpha}{2}\right) + P_c\left(V_c - \frac{\alpha}{2}\right) \tag{1}$$

$$V_c = \left(\frac{z}{h} + \frac{1}{2}\right)^k \tag{2}$$

$$V_c + V_m = 1 \Rightarrow V_c = 1 - V_m \tag{3}$$

The power law of volume fraction is described in detail in Table 1. The properties of the imperfect FGM can be formulated as

$$P = (P_c - P_m)\left(\frac{z}{h} + \frac{1}{2}\right)^k + P_m - (P_c + P_m)\frac{\alpha}{2} \tag{4}$$

The parameter k, a non-negative real number ($0 \leq k \leq \infty$), represents the volume fraction or power-law index, while z denotes the distance from the mid-plane of the beam. The FG beam transitions to a fully ceramic one as k approaches zero, and to a fully metallic one as k becomes large. The equations for Elastic Modulus (E) and the density of the material (ρ) of the imperfect FGM beam are detailed in [9]. Table 1 shows the equations used for E for the various porosity distributions present in the

Table 1 Porosity distribution in the FGM's (ceramic/metal): different types

Types	Porosity rate distribution		Elastic modulus, $E(z) =$
	Ceramic	Metal	
T-1	Perfect FG beam, without porosity ($a = 0$)		$(E_c - E_m)\left(\frac{z}{h} + \frac{1}{2}\right)^k + E_m$
T-2	50%	50%	$E_m\left(V_m - \frac{\alpha}{2}\right) + E_c\left(V_c - \frac{\alpha}{2}\right)$ $(E_c - E_m)\left(\frac{z}{h} + \frac{1}{2}\right)^k + E_m - (E_c + E_m)\frac{\alpha}{2}$
T-3	60%	40%	$E_m\left(V_m - \frac{2\alpha}{5}\right) + E_c\left(V_c - \frac{3\alpha}{5}\right)$ $(E_c - E_m)\left(\frac{z}{h} + \frac{1}{2}\right)^k + E_m - (3E_c + 2E_m)\frac{\alpha}{5}$
T-4	40%	60%	$E_m\left(V_m - \frac{3\alpha}{5}\right) + E_c\left(V_c - \frac{2\alpha}{5}\right)$ $(E_c - E_m)\left(\frac{z}{h} + \frac{1}{2}\right)^k + E_m - (2E_c + 3E_m)\frac{\alpha}{5}$
T-5	75%	25%	$E_m\left(V_m - \frac{\alpha}{4}\right) + E_c\left(V_c - \frac{3\alpha}{4}\right)$ $(E_c - E_m)\left(\frac{z}{h} + \frac{1}{2}\right)^k + E_m - (3E_c + E_m)\frac{\alpha}{4}$
T-6	25%	75%	$E_m\left(V_m - \frac{3\alpha}{4}\right) + E_c\left(V_c - \frac{\alpha}{4}\right)$ $(E_c - E_m)\left(\frac{z}{h} + \frac{1}{2}\right)^k + E_m - (E_c + 3E_m)\frac{\alpha}{4}$

FGMs. The Poisson's ratio (ν) is assumed to remain constant. In the special case where $a = 0$, we obtain material properties corresponding to a perfect FG beam.

2.2 Theoretical Formulation

2.2.1 Assumptions

The theory operates under the following assumptions:

- Displacements are significantly smaller in magnitude compared to the height of the beam, thus resulting in infinitesimal strains.
- The displacement in the transverse direction, w, comprises two components for bending (w_b) and shear (w_s), which are both solely functions of the coordinates x and t:

$$w(x, z, t) = w_b(x, t) + w_s(x, t) \tag{5}$$

- Normal stress σ_z (in the transverse direction) is considerably smaller in magnitude compared to the in-plane stresses σ_x.
- Axial displacement u (in the x-direction), comprises extension, bending, and shear components.

$$u = u_0 + u_b + u_s \tag{6}$$

- The component of bending, u_b, is assumed to closely resemble the displacements predicted by the beam theory. Hence, u_b can be expressed as

$$u_b = -z\frac{\partial w_b}{\partial x} \tag{7}$$

- The combination of the shear component u_s with w_s results in a hyperbolic variation of shear strain γ_{xz}, causing shear stress τ_{xz} to distribute across the thickness of the beam. This distribution ensures that shear stress τ_{xz} is zero at both the top and bottom surfaces of the beam. Thus, the expression for u_s can be stated as follows:

$$u_s = -f(z)\frac{\partial w_s}{\partial x} \tag{8}$$

$$f(z) = -\frac{z}{4} + \frac{5z^3}{3h^2} \tag{9}$$

2.2.2 Constitutive Equations and Kinematics

Utilizing the formulations outlined in the previous section, the field of displacements can be derived from Eqs. (5), (6), (7), (8), and (9) as

$$u(x,z,t) = u_0(x,t) - z\frac{\partial w_b}{\partial x} - f(z)\frac{\partial w_s}{\partial x} \tag{10}$$

$$w(x,z,t) = w_b(x,t) + w_s(x,t) \tag{11}$$

The strains corresponding to the displacements in Eqs. (10) and (11) are as follows:

$$\varepsilon_x = \varepsilon_x^0 + z\,k_x^b + f(z)\,k_x^s \tag{12}$$

$$\gamma_{xz} = g(z)\,\gamma_{xz}^s \tag{13}$$

where

$$\varepsilon_x^0 = \frac{\partial u_0}{\partial x}, \quad k_x^b = -\frac{\partial^2 w_b}{\partial x^2}, \quad k_x^s = -\frac{\partial^2 w_s}{\partial x^2}, \quad \gamma_{xz}^s = \frac{\partial w_s}{\partial x} \tag{14}$$

$$g(z) = 1 - f'(z), \quad f'(z) = \frac{df(z)}{dz} \tag{15}$$

Assuming adherence to Hooke's law for the material of the FG beam, the stresses within the beam can be determined:

$$\sigma_x = Q_{11}(z)\ \varepsilon_x \tag{16}$$

$$\tau_{xz} = Q_{55}(z)\ \gamma_{xz} \tag{17}$$

$$Q_{11}(z) = E(z) \tag{18}$$

$$Q_{55}(z) = E(z)/[2(1+\nu)] \tag{19}$$

2.2.3 Motion Equations

In this context, Hamilton's principle is utilized to end up to the equations of motion, as follows [10]:

$$\delta \int_{t_1}^{t_2} (U - T)dt = 0 \tag{20}$$

Here, t represents the time, t_1 is the initial, t_2 denotes the final time, δU signifies the virtual variation of the strain energy, and δT represents the virtual variation of the kinetic energy. The variation in strain energy of the beam is

$$\begin{aligned} \delta U &= \int_0^L \int_{-h/2}^{h/2} \left(\sigma_x \delta\varepsilon_x + \tau_{xz}\delta\gamma_{xz}\right) dz dx \\ &= \int_0^L \left(N_x \delta\varepsilon_x^0 - M_x^b \delta k_x^b - M_x^s \delta k_x^s + Q_{xz}\delta\gamma_{xz}^s\right) dx \end{aligned} \tag{21}$$

where the four stress resultants can be defined as

$$\left(N_x, M_x^b, M_x^s\right) = \int_{-h/2}^{h/2} (1, z, f(z))\ \sigma_x dz \tag{22}$$

$$Q_{xz} = \int_{-h/2}^{h/2} \tau_{xz} g(z) dz \tag{23}$$

The kinetic energy variation is given by

$$\begin{aligned}\delta T = & \int_0^L \int_{-h/2}^{h/2} \rho(z)[\dot{u}\delta\,\dot{u} + \dot{w}\delta\,\dot{w}]\, dz_{ns} dx \\ = & \int_0^L \left\{ I_0[\dot{u}_0 \delta\,\dot{u}_0 + (\dot{w}_b + \dot{w}_s)(\delta\,\dot{w}_b + \delta\,\dot{w}_s)] - I_1\left(\dot{u}_0 \frac{d\delta\,\dot{w}_b}{dx} + \frac{d\,\dot{w}_b}{dx}\delta\,\dot{u}_0\right)\right. \\ & + I_2\left(\frac{d\dot{w}_b}{dx}\frac{d\delta\,\dot{w}_b}{dx}\right) - J_1\left(\dot{u}_0 \frac{d\delta\,\dot{w}_s}{dx} + \frac{d\,\dot{w}_s}{dx}\delta\,\dot{u}_0\right) + K_2\left(\frac{d\dot{w}_s}{dx}\frac{d\delta\,\dot{w}_s}{dx}\right) \\ & \left. + J_2\left(\frac{d\dot{w}_b}{dx}\frac{d\delta\,\dot{w}_s}{dx} + \frac{d\dot{w}_s}{dx}\frac{d\delta\,\dot{w}_b}{dx}\right)\right\} dx\end{aligned} \tag{24}$$

In the provided context, the dot-superscript notation means differentiation with respect to the time variable t. $\rho(z)$ represents the mass density, and the mass inertias are defined as

$$(I_0, I_1, J_1, I_2, J_2, K_2) = \int_{-h/2}^{h/2} \left(1, z, f, z^2, zf, f^2\right)\rho(z) dz \tag{25}$$

By using Eqs. (21) and (24) into Eq. (20), we have

$$\delta u_0 : \frac{dN_x}{dx} = I_0\ddot{u}_0 - I_1\frac{d\ddot{w}_b}{dx} - J_1\frac{d\ddot{w}_s}{dx} \tag{26}$$

$$\delta w_b : \frac{d^2M_b}{dx^2} = I_0(\ddot{w}_b + \ddot{w}_s) + I_1\frac{d\ddot{u}_0}{dx} - I_2\frac{d^2\ddot{w}_b}{dx^2} - J_2\frac{d^2\ddot{w}_s}{dx^2} \tag{27}$$

$$\delta w_s : \frac{d^2M_s}{dx^2} + \frac{dQ_{xz}}{dx} = I_0(\ddot{w}_b + \ddot{w}_s) + J_1\frac{d\ddot{u}_0}{dx} - J_2\frac{d^2\ddot{w}_b}{dx^2} - K_2\frac{d^2\ddot{w}_s}{dx^2} \tag{28}$$

Introducing Eqs. (22) and (23) into Eqs. (26), (27), and (28), the motion equations can be expressed as follows, in terms of u_0, w_b, w_s:

$$A_{11}\frac{\partial^2 u_0}{\partial x^2} - B_{11}\frac{\partial^3 w_b}{\partial x^3} - B_{11}^s\frac{\partial^3 w_s}{\partial x^3} = I_0\ddot{u}_0 - I_1\frac{d\ddot{w}_b}{dx} - J_1\frac{d\ddot{w}_s}{dx} \tag{29}$$

$$B_{11}\frac{\partial^3 u_0}{\partial x^3} - D_{11}\frac{\partial^4 w_b}{\partial x^4} - D_{11}^s\frac{\partial^4 w_s}{\partial x^4} = I_0(\ddot{w}_b + \ddot{w}_s) + I_1\frac{d\ddot{u}_0}{dx} - I_2\frac{d^2\ddot{w}_b}{dx^2} - J_2\frac{d^2\ddot{w}_s}{dx^2} \tag{30}$$

$$B_{11}^s\frac{\partial^3 u_0}{\partial x^3} - D_{11}^s\frac{\partial^4 w_b}{\partial x^4} - H_{11}^s\frac{\partial^4 w_s}{\partial x^4} + A_{55}^s\frac{\partial^2 w_s}{\partial x^2} = I_0(\ddot{w}_b + \ddot{w}_s) + J_1\frac{d\ddot{u}_0}{dx} - J_2\frac{d^2\ddot{w}_b}{dx^2} - K_2\frac{d^2\ddot{w}_s}{dx^2} \tag{31}$$

Where the beam stiffnesses are defined by

$$\left(A_{ij}, A_{ij}^s, B_{ij}, D_{ij}, B_{ij}^s, D_{ij}^s, H_{ij}^s\right) = \int_{-h/2}^{h/2} Q_{ij}\left(1, g^2(z), z, z^2, f(z), zf(z), f^2(z)\right)dz \tag{32}$$

2.2.4 Analytical Solution

The analytical solutions in the Navier-type format are derived for the free vibration analysis of FG beams. Following this approach, the variables (unknown displacements) are expanded into a Fourier series as follows:

$$\begin{Bmatrix} u_0 \\ w_b \\ w_s \end{Bmatrix} = \sum_{m=1}^{\infty} \begin{Bmatrix} U_m \cos(\lambda x)\, e^{i\omega t} \\ W_{bm} \sin(\lambda x)\, e^{i\omega t} \\ W_{sm} \sin(\lambda x)\, e^{i\omega t} \end{Bmatrix} \tag{33}$$

In the above, U_m, W_{bm}, and W_{sm} denote arbitrary parameters that are to be calculated, ω is the frequency associated with the m-th eigenmode, and $\lambda = m{\cdot}\pi/L$. By substituting Eq. (33) into Eqs. (29), (30), and (31), the analytical solution can be derived through the eigenvalue equations below, for any given value of the eigenmode m.

$$\left([K] - \omega^2[M]\right)\{\Delta\} = \{0\} \tag{34}$$

$$[K] = \begin{bmatrix} a_{11} & a_{12} & a_{13} \\ a_{12} & a_{22} & a_{23} \\ a_{13} & a_{23} & a_{33} \end{bmatrix}, \tag{35}$$

$$[M] = \begin{bmatrix} m_{11} & m_{12} & m_{13} \\ m_{12} & m_{22} & m_{23} \\ m_{13} & m_{23} & m_{33} \end{bmatrix}, \tag{36}$$

$$\{\Delta\} = \begin{Bmatrix} U_m \\ W_{bm} \\ W_{sm} \end{Bmatrix}, \tag{37}$$

$$a_{11} = A_{11}\lambda^2, \quad a_{12} = -B_{11}\lambda^3, \quad a_{13} = -B^s_{11}\lambda^3, \tag{38}$$

$$a_{22} = D_{11}\lambda^4, \quad a_{23} = D^s_{11}\lambda^4, \quad a_{33} = H^s_{11}\lambda^4 + A^s_{55}\lambda^2 \tag{39}$$

$$m_{11} = I_0, \quad m_{12} = -I_1\alpha, \quad m_{13} = -J_1\alpha, \tag{40}$$

$$m_{22} = I_0 + I_2\alpha^2, \quad m_{23} = I_0 + J_2\alpha^2, \quad m_{33} = I_0 + K_2\alpha^2 \tag{41}$$

3 Results

We present the results for the numerical frequencies of imperfect FGM beams with various rates of porosity distribution, with the aim of validating the accuracy of the present formulation. The properties of the beam's material are outlined below:

- Ceramic part: Al_2O_3 (Alumina) with $\nu = 0.3$, $E_c = 380$ GPa, $\rho = 3960$ kg/m^3.
- Metal part: Al (Aluminum) with $\nu = 0.3$, $E_m = 70$ GPa, $\rho = 2702$ kg/m^3.

The following non-dimensional parameter has been used for simplicity:

$$\overline{\omega} = \frac{\omega \cdot L^2}{h}\sqrt{\frac{\rho_m}{E_m}} \tag{42}$$

The natural frequencies of both imperfect and perfect beams were examined for $L/h = 5$ and $L/h = 20$ across various power-law indices (k), with results summarized in Table 2. The present theory's outcomes are corroborated and demonstrate excellent alignment with previously published findings. Additionally, the analysis extends to different porosity types categorized as T-1 to T-6, as detailed in Table 1. The results reveal that the natural frequency attains its maximum for T-6, followed by the cases T-4, T-2, T-3, T-5, and T-1.

When the beam is composed entirely of ceramic ($k = 0$), an escalation in grading indices results in a greater proportion of metal within the beam, consequently diminishing its stiffness and subsequently reducing its natural frequency. This trend mirrors the behavior observed in the non-dimensional flexural natural frequencies of porous functionally graded beams, as depicted in Table 3 (for $L/h = 5$) and Table 4 (for $L/h = 20$). Across all instances, the natural frequency is higher for porous beams in comparison to non-porous beams.

Figure 1 shows the evolution of the frequency of imperfect FG beams across a range of power-law indices (k). The analysis reveals a decline in frequency with the augmentation of the porosity fraction k. Specifically, when k is less than 5, a sharp

Table 2 Non-dimensional frequencies of simply supported porous FG beams ($a = 0.1$)

L/h	Theory	$k = 0$	$k = 1$	$k = 2$	$k = 5$	$k = 10$
5	Bernoulli–Euler (1744) [11]	5.3953	4.1484	3.7793	3.5949	3.4921
	Timoshenko (1921) [12]	5.1524	3.9902	3.6343	3.4311	3.3134
	Simsek (2010) [13]	5.1527	3.9904	3.6261	3.4012	3.2816
	Reddy (1984) [14]	5.1527	3.9904	3.6264	3.4012	3.2816
	Sayyad et al. (2018) [15]	5.1453	3.9826	3.6184	3.3917	3.2727
	T-1	5.1527	3.9904	3.6264	3.4012	3.2816
	T-2	5.2223	3.9070	3.4418	3.1479	3.0292
	T-3	5.2087	3.8712	3.3889	3.0813	2.9627
	T-4	5.2359	3.9419	3.4928	3.2113	3.0924
	T-5	5.1879	3.8158	3.3058	2.9745	2.8561
	T-6	5.2559	3.9929	3.5659	3.3011	3.1819
20	Bernoulli–Euler (1744) [11]	5.4777	4.2163	3.8472	3.6628	3.5547
	Timoshenko (1921) [12]	5.4603	4.2050	3.8367	3.6508	3.5415
	Simsek (2010) [13]	5.4603	4.2050	3.8361	3.6485	3.5389
	Reddy (1984) [14]	5.4603	4.2050	3.8361	3.6485	3.5389
	Sayyad et al. (2018) [15]	5.4603	4.2050	3.8361	3.6485	3.5389
	T-1	5.4603	4.2051	3.8361	3.6485	3.5389
	T-2	5.5341	4.1117	3.6335	3.3776	3.2809
	T-3	5.5196	4.0732	3.5764	3.3059	3.2113
	T-4	5.5484	4.1494	3.6885	3.4458	3.3470
	T-5	5.4976	4.0137	3.4866	3.1907	3.0993
	T-6	5.5696	4.2042	3.7674	3.5421	3.4405

Table 3 Flexural natural frequencies (non-dimensional) of porous FG beams ($a = 0.1$, $L/h = 5$)

Mode	Theory	$k = 0$	$k = 1$	$k = 2$	$k = 5$	$k = 10$
1	Sayyad et al. (2018) [15]	5.1453	3.9826	3.6184	3.3917	3.2727
	T-1	5.1527	3.9904	3.6264	3.4012	3.2816
	T-2	5.2223	3.9070	3.4418	3.1479	3.0292
	T-3	5.2087	3.8712	3.3889	3.0813	2.9627
	T-4	5.2359	3.9419	3.4928	3.2113	3.0924
	T-5	5.1879	3.8158	3.3058	2.9745	2.8561
	T-6	5.2559	3.9929	3.5659	3.3011	3.1819
2	Sayyad et al. (2018) [15]	17.589	13.754	12.388	11.260	10.748
	T-1	17.881	14.009	12.641	11.543	11.024
	T-2	18.123	13.755	12.049	10.685	10.103
	T-3	18.075	13.635	11.873	10.462	9.870
	T-4	18.169	13.873	12.219	10.898	10.326
	T-5	18.003	13.449	11.596	10.106	9.497
	T-6	18.239	14.044	12.463	11.202	10.642
3	Sayyad et al. (2018) [15]	32.324	25.538	22.812	20.117	19.003
	T-1	34.209	27.098	24.315	21.716	20.556
	T-2	34.672	26.675	23.276	20.124	18.748
	T-3	34.581	26.453	22.953	19.711	18.301
	T-4	34.761	26.892	23.587	20.519	19.175
	T-5	34.443	26.109	22.446	19.056	17.589
	T-6	34.895	27.209	24.035	21.082	19.783

Table 4 Non-dimensional flexural natural frequencies of porous FG beams ($a = 0.1$, $L/h = 20$)

Mode	Theory	$k = 0$	$k = 1$	$k = 2$	$k = 5$	$k = 10$
1	Sayyad et al. (2018) [15]	5.4603	4.2050	3.8361	3.6484	3.5389
	T-1	5.4603	4.2051	3.8361	3.6485	3.5389
	T-2	5.5341	4.1117	3.6335	3.3776	3.2809
	T-3	5.5196	4.0732	3.5764	3.3059	3.2113
	T-4	5.5484	4.1494	3.6885	3.4458	3.3470
	T-5	5.4976	4.0137	3.4866	3.1907	3.0993
	T-6	5.5696	4.2042	3.7674	3.5421	3.4405
2	Sayyad et al. (2018) [15]	21.571	16.631	15.158	14.370	13.922
	T-1	21.573	16.634	15.162	14.375	13.926
	T-2	21.865	16.270	14.367	13.306	12.898
	T-3	21.807	16.118	14.143	13.024	12.622
	T-4	21.921	16.418	14.584	13.575	13.159
	T-5	21.721	15.884	13.789	12.571	12.178
	T-6	22.005	16.634	14.895	13.954	13.530
3	Sayyad et al. (2018) [15]	47.569	36.740	33.440	31.543	30.505
	T-1	47.593	36.768	33.469	31.578	30.537
	T-2	48.236	35.979	31.737	29.228	28.239
	T-3	48.109	35.646	31.245	28.609	27.628
	T-4	48.361	36.304	32.211	29.818	28.819
	T-5	47.918	35.131	30.470	27.615	26.646
	T-6	48.546	36.778	32.893	30.652	29.642

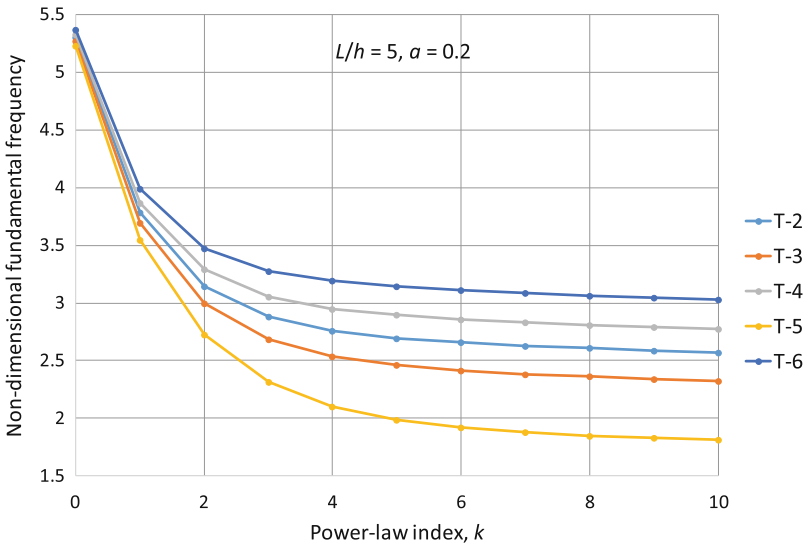

Fig. 1 Fundamental frequency $\overline{\omega}$ of imperfect beams versus power-law index, k ($L/h = 5$, $a = 0.2$)

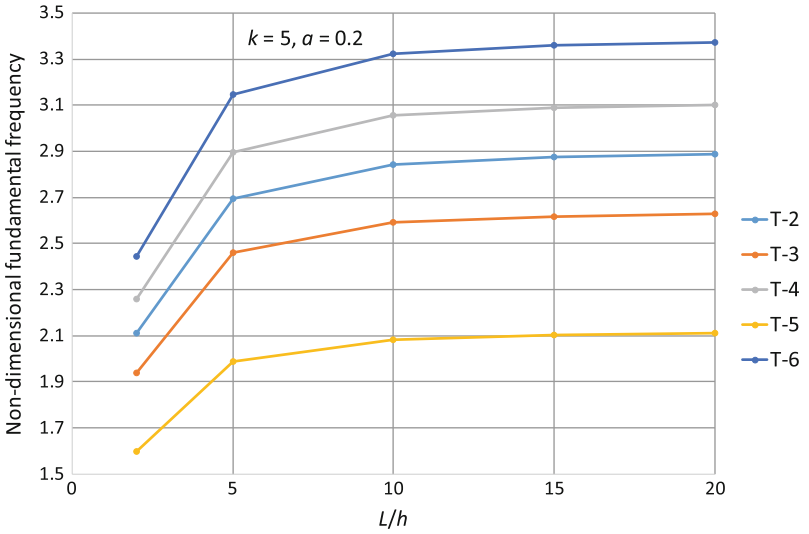

Fig. 2 Fundamental frequency $\overline{\omega}$ of imperfect beams versus L/h ratio ($k = 5$, $a = 0.2$)

decrease in frequency occurs, whereas beyond k greater than 5, a consistent decrease in natural frequency is observed. Furthermore, the investigation into natural frequency encompassed various L/h ratios and different porosity types, demonstrating an increase in frequency with higher L/h ratios (Fig. 2).

4 Conclusions

This study conducted a comprehensive analysis of the free vibration behavior of FG beams with porosities, considering various types of porosity. The investigation focused on evaluating the impact of differing levels of porosity within ceramic and metal components. Specifically, the analysis examined how the power-law index, length-to-thickness ratio, and porosity distribution types influenced the natural frequency.

Validation of the obtained results was performed by comparing them with existing literature for cases where the beam exhibited no porosity. The findings revealed that an increase in the power-law indices resulted in a decrease in the stiffness of functionally graded beams, leading to a corresponding reduction in natural frequency. Additionally, it was observed that a higher length-to-thickness ratio (L/h ratio) was associated with an increase in natural frequency.

Furthermore, the study demonstrated a significant decrease in the natural frequency as the percentage of porosity increased, regardless of the specific porosity types examined. These findings provide valuable insights for industries engaged in the manufacturing of porous beams, aiding in the decision-making process for

selecting the most suitable porosity type to achieve optimal performance objectives. Overall, this analysis contributes to advancing our understanding of the complex interplay between porosity, material properties, and geometric parameters in functionally graded structures, with implications for various engineering applications.

References

1. Abdelall, E.S., Hayajneh, M., Almomani, M.: Fabrication of functionally graded injection molds using friction stir molding process of AA5083/brass-laminated composite. Prog. Addit. Manuf. **8**(2), 169–177 (2023). https://doi.org/10.1007/s40964-022-00320-8
2. Adachi, T., Higuchi, M.: Fabrication of bulk functionally-graded syntactic foams for impact energy absorption. Mater. Sci. Forum. **706–709**, 711–716 (2012). https://doi.org/10.4028/www.scientific.net/MSF.706-709.711
3. Boss, J.N., Ganesh, V.K.: Fabrication and properties of graded composite rods for biomedical applications. Compos. Struct. **74**(3), 289–293 (2006). https://doi.org/10.1016/j.compstruct.2005.04.030
4. Al Jahwari, F., Anwer, A.A.W., Naguib, H.E.: Fabrication and microstructural characterization of functionally graded porous acrylonitrile butadiene styrene and the effect of cellular morphology on creep behavior. J. Polym. Sci. B Polym. Phys. **53**(11), 795–803 (2015). https://doi.org/10.1002/polb.23698
5. Arefi, M., Firouzeh, S., Mohammad-Rezaei Bidgoli, E., Civalek, Ö.: Analysis of porous microplates reinforced with FG-GNPs based on Reddy plate theory. Compos. Struct. **247**, 112391 (2020). https://doi.org/10.1016/j.compstruct.2020.112391
6. Madan, R., Bhowmick, S.: Fabrication and microstructural characterization of Al-SiC based functionally graded disk. Aircr. Eng. Aerosp. Technol. **95**(2), 292–301 (2023). https://doi.org/10.1108/AEAT-03-2022-0096
7. Hadji, L., Plevris, V., Madan, R.: A static and free vibration analysis of porous functionally graded beams. In: 2nd International Conference on Civil Infrastructure and Construction (CIC 2023). QU Press, Doha, Qatar (2023). https://doi.org/10.29117/cic.2023.0059
8. Wattanasakulpong, N., Ungbhakorn, V.: Linear and nonlinear vibration analysis of elastically restrained ends FGM beams with porosities. Aerosp. Sci. Technol. **32**(1), 111–120 (2014). https://doi.org/10.1016/j.ast.2013.12.002
9. Zouatnia, N., Hadji, L., Kassou, A.: An analytical solution for bending and vibration responses of functionally graded beams with porosities. Wind Struct. **25**(4), 329–342 (2017). https://doi.org/10.12989/was.2017.25.4.329
10. Thai, H.-T., Vo, T.P.: Bending and free vibration of functionally graded beams using various higher-order shear deformation beam theories. Int. J. Mech. Sci. **62**(1), 57–66 (2012). https://doi.org/10.1016/j.ijmecsci.2012.05.014
11. Euler, L.: Methodus inveniendi lineas curvas maximi minimive proprietate gaudentes, sive solutio problematis isoperimetrici lattissimo sensu accepti, vol. 24. 1744, pp. 1–308. apud Marcum-Michaelem Bousquet & Socios, Lausannae & Genevae
12. Timoshenko, S.P.: LXVI. On the correction for shear of the differential equation for transverse vibrations of prismatic bars. Lond. Edinb. Dublin Philos. Mag. J. Sci. **41**(245), 744–746 (1921). https://doi.org/10.1080/14786442108636264
13. Şimşek, M.: Fundamental frequency analysis of functionally graded beams by using different higher-order beam theories. Nucl. Eng. Des. **240**(4), 697–705 (2010). https://doi.org/10.1016/j.nucengdes.2009.12.013

14. Reddy, J.N.: A simple higher-order theory for laminated composite plates. J. Appl. Mech. **51**(4), 745–752 (1984). https://doi.org/10.1115/1.3167719
15. Sayyad, A.S., Ghugal, Y.M.: An inverse hyperbolic theory for FG beams resting on Winkler-Pasternak elastic foundation. Adv. Aircraft Spacecraft Sci. **5**(6), 671–689 (2018). https://doi.org/10.12989/aas.2018.5.6.671